

Continuous precipitation of ceria nanoparticles from a continuous flow micromixer

Chih Heng T. Tseng · Brian K. Paul ·
Chih-Hung Chang · Mark H. Engelhard

Received: 22 September 2011 / Accepted: 18 June 2012 / Published online: 14 August 2012
© Springer-Verlag London Limited 2012

Abstract Cerium oxide nanoparticles were continuously precipitated from a solution of cerium(III) nitrate and ammonium hydroxide using a static microchannel T-mixer. T-mixer synthesis results were compared with synthesis results from batch precipitation. Findings show that the method of mixing is important in the ceria precipitation process. Uniform porous film structures and nanorods were produced when the particle chemistry was synthesized using T-mixing followed by spin coating. Batch mixing, when using higher NH_4OH feed concentrations followed by spin coating, was characterized by the heavy agglomeration of nanoparticles. Similar, high aspect ratio nanorods were produced when feed conditions in both batch mixing and T-mixing were identical demonstrating that the momentum effects of continuous microchannel T-mixing did not impact the synthesis process. In addition, it was found that the micromixing approach reduced the exposure of the $\text{Ce}(\text{OH})_3$ precipitates to oxygen, yielding hydroxide precipitates in place of CeO_2 precipitates. The key advantage of the micro-scale T-mixing approach is higher throughput which is important for the scaling of ceria nanoparticle production.

Keywords Continuous flow synthesis · Ceria · Nanoparticles · Microreactor · Micromixer

1 Introduction

Cerium dioxide (CeO_2) has drawn much attention in recent years due to its distinctive characteristics, such as unique UV absorptivity [1], high stability and hardness at high temperature, and high reactivity to oxygen [2]. Unique optical characteristics such as Raman-allowed modes shifting and broadening [3], lattice expansion, and the blue shift in ultraviolet absorption spectra [4] have been reported. Catalytic applications such as support or promoter for exhaust-gas conversion (three-way catalyst application) [5], oxygen ion conductor in fuel cells [6], and gas sensors [7] have also been reported.

With such a variety of applications, different forms (particle, mesoporous membrane/film, or composite membrane/film) of CeO_2 have been proposed and analyzed. In particular, CeO_2 nanoparticles have been greatly exploited because of the significant size-induced property changes [7]. In oxygen sensor applications, by changing the particle size from micrometers to hundreds of nanometers, the response time shortened from minutes to milliseconds [8]. Moreover, nanocrystalline CeO_2 particles have allowed 200–400 °C decreases in sintering temperature when compared with micron-sized CeO_2 particles [9]. To facilitate the application of ceria nanoparticles in the marketplace, it is important to identify a way to scale the synthesis of ceria nanoparticles.

Over the past few years, several methods have been proposed for synthesizing CeO_2 nanoparticles including sol-gel [10, 11], hydrothermal or solvothermal [12, 13], forced hydrolysis [14], microemulsion [15] and precipitation [16–18] among others. Precipitation is an attractive route due to cheap salt precursors and low-temperature operation [19]. To date, most research on nanoparticle

C. H. T. Tseng · B. K. Paul (✉)
School of Mechanical, Industrial, and Manufacturing Engineering,
Oregon State University,
204 Rogers Hall,
Corvallis, OR 97331, USA
e-mail: brian.paul@oregonstate.edu

C.-H. Chang
School of Chemical, Biological, and Environmental Engineering,
Oregon State University,
313 Gleeson Hall,
Corvallis, OR 97331, USA

M. H. Engelhard
Environmental Molecular Sciences Laboratory, Pacific Northwest
National Laboratory,
P.O. Box 999, K8-87,
Richland, WA 99352, USA

precipitation has focused on the use of surfactants to slow down the release of reactants and thereby reduce the reaction time or to alter the reactant concentration or dielectric constant. By lengthening the reaction time, effects due to poor mass transfer during batch mixing can be minimized.

In contrast, micromixers offer the possibility of reducing reaction times by reducing diffusional distances allowing for higher throughput and better process control [20, 21]. The large surface area-to-volume ratios within microchannel structures lead to accelerated heat and mass transport. This accelerated transport allows for rapid changes in reaction temperatures and concentrations leading to more uniform heating and mixing [22]. Consequently, micromixers have been demonstrated to have dramatic impacts on macromolecular yields [23, 24] and nanoparticle size distributions [25–28]. In addition, the use of microchannels provides a means for scaling up production by “numbering up” [29]. “Numbering up” involves increasing the volumetric flow rate through increases in flow cross section by adding parallel microchannels. In this manner, flow reaction conditions remain unchanged in each individual microchannel as the process is increased in scale.

Prior work has focused on demonstrating ceria nanoparticle synthesis from a continuous flow microreactor [30]. In this paper, we analyze the products from the continuous precipitation of CeO₂ nanorods using a continuous flow static microchannel T-mixer and compare the results with those produced using batch reactor methods. Not only do microchannel mixers provide higher throughput, but, as will be shown, they also provide a means for shielding the nanoparticles from environmental contamination during synthesis.

2 Experimental approach

A conventional batch mixing strategy for ceria precipitation (shown in Fig. 1a) involves pipetting ammonium hydroxide (NH₄OH) into an aqueous solution of cerium(III) nitrate until the pH rises above 10. At that point, supersaturation leads to the nucleation of ceria precipitates followed by particle growth. In this case, the supersaturation value, S , is defined as:

$$S = \frac{[\text{Ce}^{3+}] \cdot [\text{OH}^-]^3}{K_{\text{SP}}} \quad (1)$$

where $[\text{Ce}^{3+}]$ and $[\text{OH}^-]$ are the cerium and hydroxyl ion concentrations and K_{sp} is the solubility product constant for cerium hydroxide, respectively. In theory, higher supersaturation values should result in more nucleation sites and smaller precipitate sizes. In this case, the supersaturation value is highly dependent upon increases in $[\text{OH}^-]$ species.

In this experiment, batch mixing and micromixing strategies were compared by implementing two sets of recipes based on the work of Chang and Chen [31]. For batch mixing, reactants were mixed in a beaker using a magnetic stirrer at 500 RPM. The two batch mixing recipes are shown in Fig. 1b. Experiment (1) involved mixing 0.0375 M (moles solute per liter of solution) of cerium nitrate (molar mass of 434.22 g/mole) with 3 mL of 5 N (normal=molarity of base times the number of hydroxyl ions) NH₄OH pipetted in increments of 250 μL. This nitrate concentration is one half of that used by Chang and Chen. This was necessary since higher concentrations caused clogging problems in the T-mixer. For experiment (2), 0.0187 M of cerium nitrate was mixed with 5 mL of 5 N NH₄OH pipetted in increments of 250 μL.

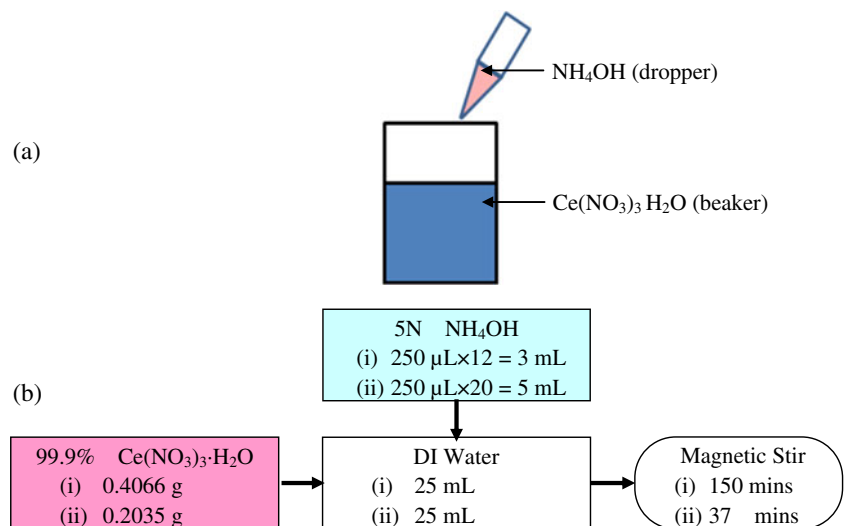
The protocol for the micromixing approach involved the use of a T-mixer in line with a single peristaltic pump as shown in Fig. 2a. The peristaltic pump was used to pump aqueous solutions of cerium(III) nitrate and dilute ammonium hydroxide through the T-mixer. After mixing, the reaction was quenched in a beaker with 50 mL of deionized water.

Two similar mixing experiments were conducted using the T-mixing approach. For experiment (1), 0.0375 M of cerium nitrate was introduced on one side, and 3 mL of dilute NH₄OH was introduced on the other side of the T-mixer. For experiment (2), 0.0187 M of cerium nitrate was used, and 5 mL of dilute NH₄OH was applied (Fig. 2b.). Overall, the amount of reactants and solvents used in the T-mixing approach was the same as the batch recipe. However, the concentrations of reactants were different due to the constraint of needing identical volumetric flow rates through the T-mixer. Subsequently, a second set of experiments was conducted as shown in Fig. 3. These experiments used identical concentration conditions.

To characterize the morphology of the nanoparticles and the elemental distribution of the deposited thin films, a Zeiss Ultra scanning electron microscope (SEM) with energy-dispersive X-ray spectroscopy (EDS) was used. The samples for SEM study were applied to a 25×25-mm microscope glass slide by spin coating. The spin coating process was carried out in two sequential steps. First, samples were spun at 500 rpm (100 rpm/s acceleration) for 10 s. During this step, about 4 mL of the product solution was slowly dropped onto the substrate. For the second step, the samples were ramped up to 1,500 rpm (300 rpm/s acceleration) and held for 30 s to discard excess colloidal solution and accelerate the evaporation of deionized (DI) water. The coated glass slides were then heated in a hot plate oven at 95 °C for 14 h.

The chemistry of the deposited nanoparticles was characterized by X-ray photon spectroscopy (XPS). To prepare

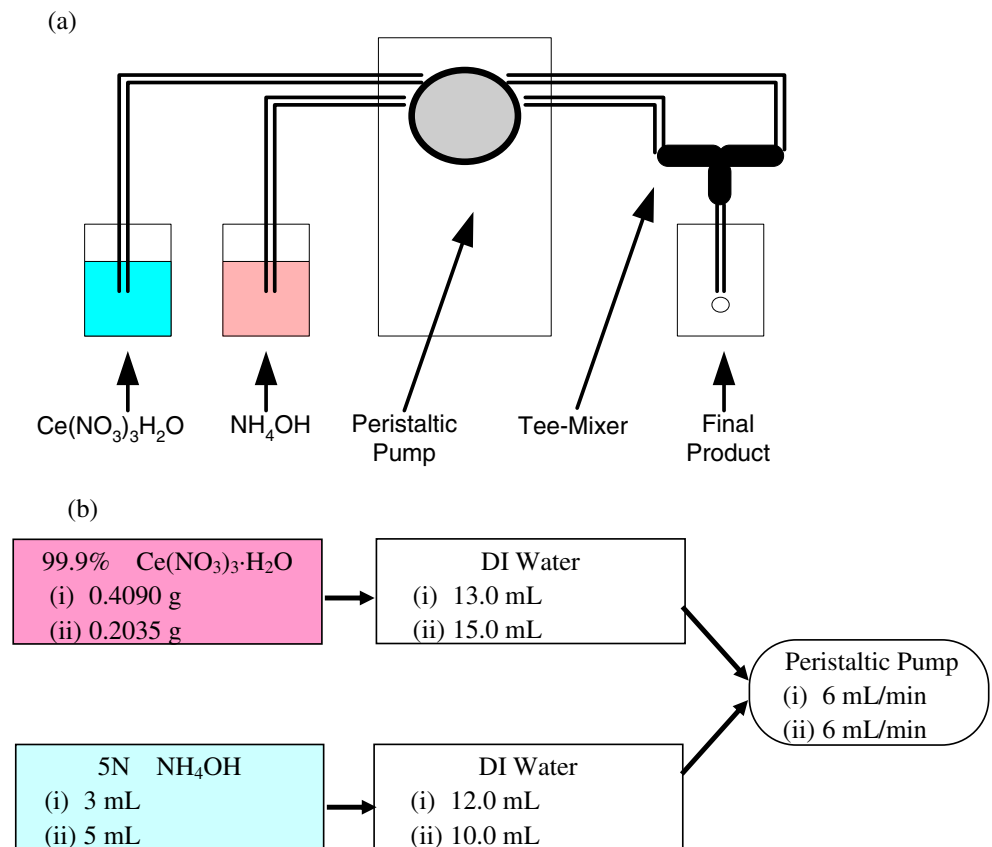
Fig. 1 a Schematic diagram of the batch mixing approach. b Batch mixer precipitation protocols



the XPS sample, the mixed solutions were deposited by pipette onto a clean Si wafer inside a nitrogen-purged I²R glove bag attached to the XPS sample introduction chamber. The DI water in the solution was allowed to dry for approximately 10 min while inside the N₂-purged glove bag. The samples were mounted onto the XPS system specimen holder, and XPS measurements were performed using a Physical Electronics Quantum 2000 Scanning ESCA Microprobe (Environmental Molecular Sciences Laboratory, Pacific

Northwest National Laboratory, Richland, WA). This system uses a focused monochromatic Al K α X-rays (1,486.7 eV) source and a spherical section analyzer. The instrument has a 16-element multichannel detector. The X-ray beam used was a 100-W, 100- μm diameter beam that was rastered over a 1.3 \times 0.2-mm rectangle on the sample. A transmission electron microscope (TEM=FEI Tecnai F-20 field emission high resolution) was used to study particle formation. In the preparation of TEM samples, copper grids

Fig. 2 a Schematic diagram of the T-mixing approach setup, b micromixer precipitation protocols



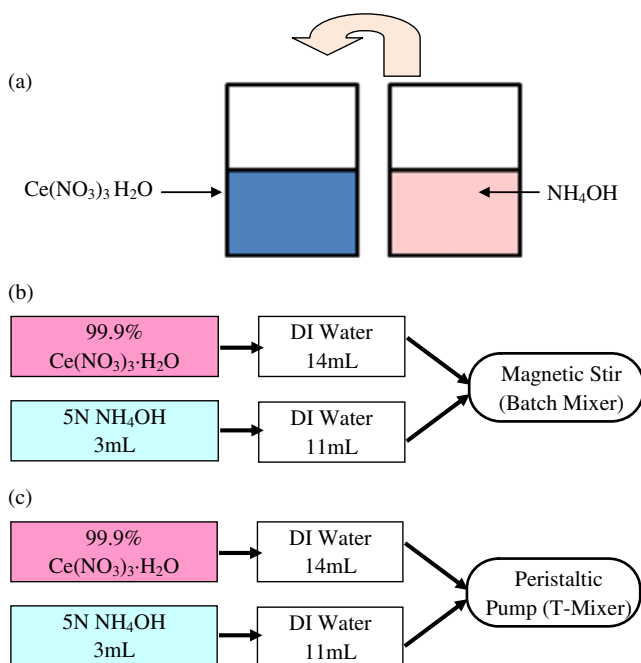


Fig. 3 **a** Schematic diagram of the alternative batch mixing approach, **b** the alternative batchmixing precipitation procedure, **c** T-mixer precipitation protocol for comparison

(with thin lacey carbon films) were dipped into the mixed solution for about 20 s after mixing was completed.

3 Results and discussions

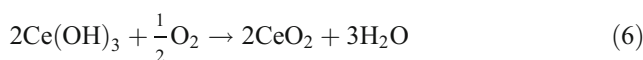
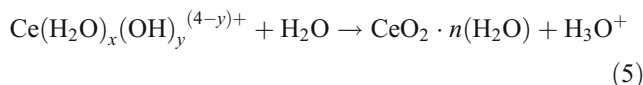
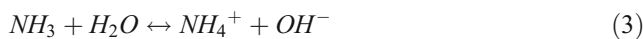
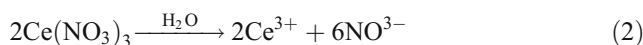
In batch mixing experiments (1) and (2), a light yellow solution was formed after mixing for 162 and 37 min, respectively. After roughly 25 min of magnetic stirring, the color of the solution appeared yellowish purple. In general, the state of oxidation in a ceria precipitation reaction can be visually identified by the light purple color of $\text{Ce}(\text{OH})_3$ and the light yellow color of CeO_2 [31]. With flow rates of 6 mL/min, the T-mixer finished the process in 4.7 and 5 min, respectively, yielding a solution that was light purple in color (Fig. 4). These results demonstrate 34.5 times and 7.4 times increases in throughput.

The process of precipitating ceria starts with dissolving cerium nitrate in DI water expressed in Eq. 2. Since the desired final product is CeO_2 , the Ce^{3+} ion must go through an oxidation transition to a Ce^{4+} ion. Chen et al. [17] suggested that a basic solution favors Ce^{4+} compared to Ce^{3+} . To increase the pH value (and, therefore, facilitate the oxidation process), ammonium hydroxide is added to the aqueous solution. Resultant ammonia molecules are protonated to form ammonium and hydroxyl ions (Eq. 3). As pH changes, $\text{Ce}(\text{OH})_3$ (cerium(III) hydroxide) quickly precipitates out due to an extremely low solubility constant ($K_{\text{sp}} = 6.3 \times 10^{-24}$ at 25 °C) [30]. This is



Fig. 4 Results from experiment (1) for batch (left) and T-mixer (right)

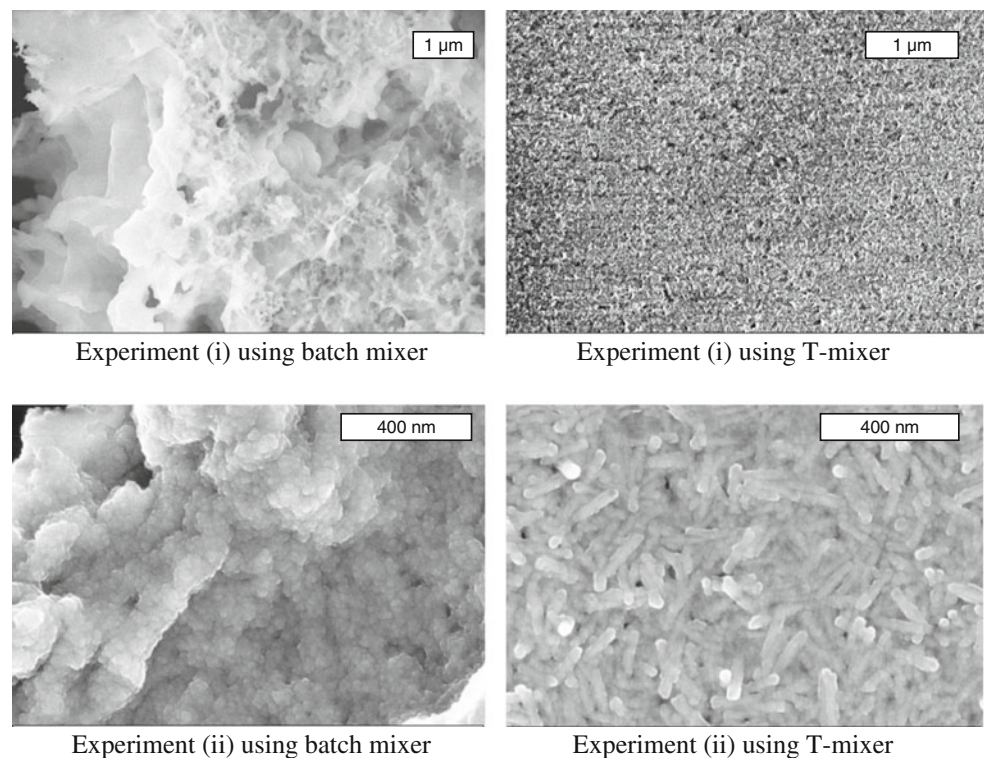
a thermodynamically driven phenomenon (Eq. 4). The cerium hydroxide then experiences a $\text{Ce}^{3+}/\text{Ce}^{4+}$ transition. Afterwards, the Ce^{4+} ions usually undergo strong hydration due to its lower alkalinity and higher charge. The hydrated Ce^{4+} ions can form complexes with water molecules or OH^- ions, in the form of $\text{Ce}(\text{H}_2\text{O})_x(\text{OH})_y^{(4-y)+}$, where $x+y$ is the coordination number of Ce^{4+} . In aqueous solution, this becomes the precursor for the CeO_2 because H_2O tends to take protons away from the hydroxide. This is expressed in Eq. 5. Zhou et al. [19] further proved that the size of CeO_2 particles can be changed by introducing oxygen bubbles into the solution to react with $\text{Ce}(\text{OH})_3$. This reaction is expressed in Eq. 6.



In batch mixing, the solution was exposed to the ambient environment for a much longer time than for the micromixer. Consequently, we believe this led to the conversion of $\text{Ce}(\text{OH})_3$ to CeO_2 which would explain the different color products.

SEM images (Fig. 5) show significant differences in the morphologies of deposited nanoparticle films. All films were found to be discontinuous. However, the film structure produced using the batch-mixed solution was found to be

Fig. 5 Comparison of morphology by different synthesis approach and concentration



agglomerated and unordered. SEM images of films produced using the T-mixer show more uniform, porous films and nanorod structures.

The formation of nanorods is not fully understood for ceria precipitation. Yamashita et al. [32] has shown that in order to precipitate nanorods, $[\text{OH}^-]$ have to be above a certain value. Results from Chang and Chen [31] suggest that ceria nanorod formation happens by two-stage non-isothermal precipitation. Our study shows that nanorods are also attainable at room temperature. Since the samples prepared for the SEM study did not go through a calcination process, the results suggest that the nanorod structure was formed before the deposition process. One possibility for the formation of the nanorod might be preferred agglomeration due to the nanoparticle shape. Recent studies suggest that the particles tend to form a coherent interface as a result of minimizing interface energy [33], leading possibly to a preferred orientation in particle orientation. Another possibility is that the nanorods are formed by the rolling of laminar structures similar to the formation of carbon nanotubes [34].

The results from the first set of batch and T-mixing experiments indicate that mixing plays a crucial role in the ceria precipitation process. To further investigate these phenomena, experimental protocols were changed to use identical reactant concentrations. For batch mixing, cerium(III) nitrate and ammonium hydroxide were both diluted in DI water. The volume and concentrations of reactants for batch mixing were matched with those of T-mixing (Fig. 3).

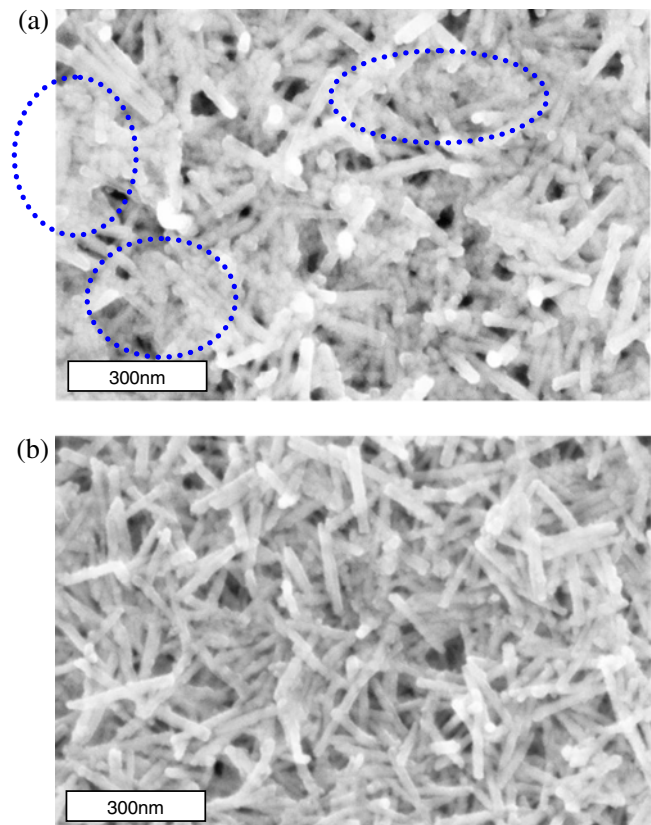


Fig. 6 **a** SEM image of nanoparticle morphology synthesized using batch precipitation approach. The *circles* indicate breakage of nanorods into nanoparticles. **b** SEM image of nanoparticle morphology synthesized using T-mixer precipitation approach

Fig. 7 Data summary showing differences of nanorod diameter and length

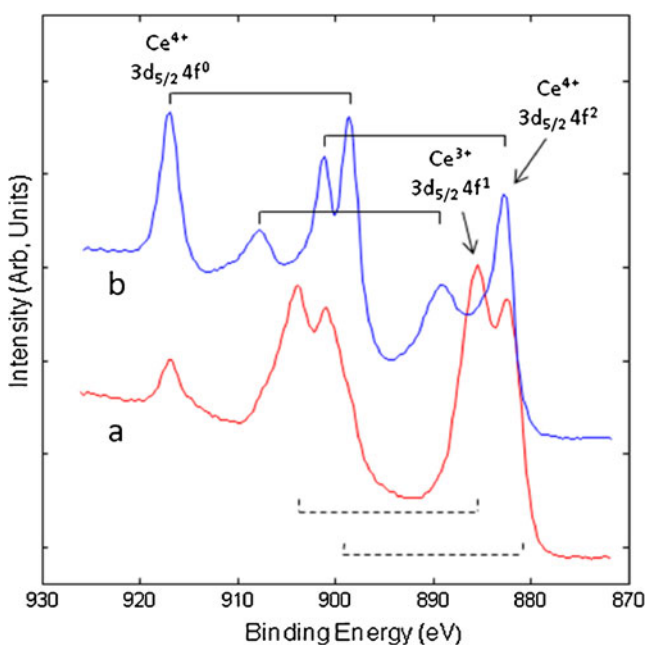
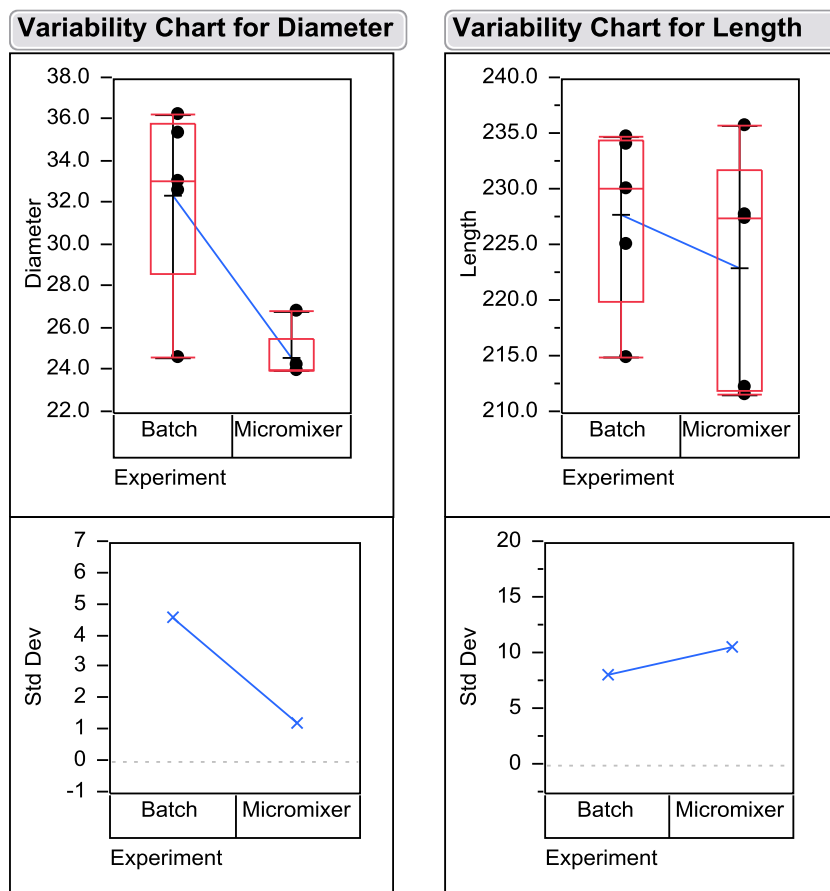


Fig. 8 XPS high energy resolution photoemission spectra of the Ce 3d region. *a* T-mixer, *b* batch mixer. The brackets in Fig. 6 show the spin orbital pairs (5/2 and 3/2) for Ce^{4+} (solid lines) and Ce^{3+} (dashed lines)

Again, for batch mixing, the reactants were mixed using a magnetic stirrer at 500 rpm.

Both SEM images (Fig. 6) reveal nanorod structures. Quartz PCI software was used to analyze the size distribution which is summarized in Fig. 7. Nanorod lengths were found to be roughly equivalent at 223.0 ± 10.6 and $227.8 \pm$

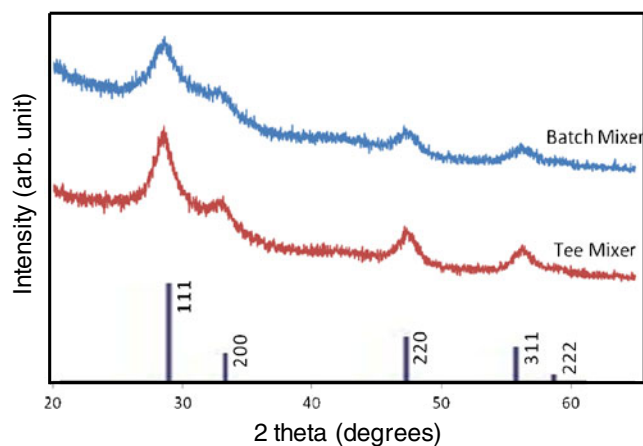


Fig. 9 Powder XRD pattern of the product compared with reference to CeO_2 JCPDS (Joint Committee on Powder Diffraction Standards) CAS (Chemical Abstracts Service) #810792

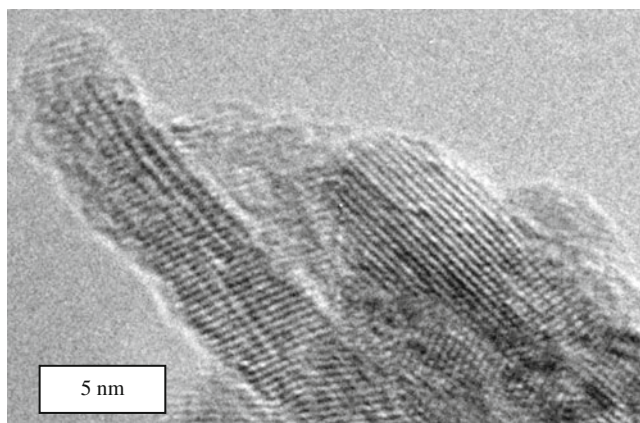


Fig. 10 TEM images of nanoparticles synthesized from T-mixer

8.1 nm for the micromixing and batch approaches, respectively. However, the average diameters were found to be 24.7 ± 1.2 and 32.4 ± 4.6 nm for the micromixing and batch approaches, respectively, showing that the batch approach yielded nanorods with 31 % larger diameters having almost $4 \times$ the variability. Consequently, aspect ratios for micromixing-assisted synthesis were found to be over 9:1 compared with approximately 7:1 for batch synthesis. Further, batch nanorods also appear to be interspersed with clusters of nanoparticles as shown in Fig. 6. In prior work, similar disintegration of ceria nanorods into nanoparticles has been observed after batch mixing and hydrothermal treatments which could be attributed to turbulence during batch mixing [35].

As hypothesized earlier, it is expected that the micromixing approach reduced the exposure of the reacting flux to oxygen thus yielding more Ce^{3+} ions which form the intermediate $\text{Ce}(\text{OH})_3$ instead of CeO_2 . To quantify the results, an X-ray photoelectron spectroscopy (XPS) analysis was performed. Nanoparticles were deposited by pipette onto clean Si wafers inside a nitrogen-purged I²R glove bag attached to the XPS sample introduction chamber. The resultant solution was allowed to dry while inside the N_2 -purged glove bag. Samples were dried for approximately 10 min and mounted onto the XPS system specimen holder. XPS high energy resolution photoemission spectral plots are shown in Fig. 8. The bracketed peaks in this plot show the spin orbital pairs (5/2 and 3/2) for Ce^{4+} (solid lines) and Ce^{3+} (dashed lines). These plots clearly show more (i.e., higher intensity peaks) Ce^{3+} ions in the T-mixed sample than in the batch-mixed samples. An N1s line was found at 407 eV suggesting that NH_3 oxidized as a nitrate.

To verify the crystal structure of the nanoparticles, the resultant nanoparticles were deposited onto a glass slide, dried for 12 h at room temperature and, afterwards, characterized by X-ray diffraction (XRD). XRD patterns (Fig. 9) indicate the existence of CeO_2 (JCPDS CAS#810792) in

both batch mix and T-mix samples. Results from EDS show similar results indicating a high percentage of Ce and O. This is congruent with drying procedures which would cause any hydroxide to convert to oxides under ambient conditions.

To further investigate nanoparticle morphology and crystallinity, a transmission electron microscope (TEM) was used to analyze resultant nanorod configurations. Samples were prepared by depositing the resultant solution onto a TEM copper grid followed by drying at room temperature for 12 h. High-resolution TEM images (Fig. 10) of T-mixed nanorods show uniform and repeatable atomic structures representative of a single crystal. EDS data from the TEM show similar results to those from the SEM with the exception of increased copper content due to the copper grid.

4 Conclusions

Results from batch mixed and T-mixed protocols show that unoptimized micromixing was from 7 to 34 times faster than batch mixing. At higher NH_4OH concentrations, batch mixing and deposition was characterized by the heavy agglomeration of nanoparticles. At lower NH_4OH concentrations, batch and T-mixed protocols were characterized by nanorods. In addition, it was found that the T-mixer permitted the formation and capture of an unstable intermediate $\text{Ce}(\text{OH})_3$ molecule by shielding the intermediate from exposure to the oxygen environment. Future work should investigate the effects of different mixing and heating strategies on the nanoparticle size, shape, and phase of ceria nanoparticles.

Acknowledgments This research was funded by the DARPA RIMS program and National Science Foundation under grant CBET-0654434. The authors would like to thank Dr. Chunfei Li at PSU for his assistance in obtaining the TEM images. The XPS portion of this manuscript was performed using EMSL, a national scientific user facility sponsored by the Department of Energy's Office of Biological and Environmental Research located at Pacific Northwest National Laboratory.

References

1. Tsunekawa S, Kasuya A (2000) Blue shift in ultraviolet absorption spectra of monodisperse CeO nanoparticles. *J Appl Phys* 87:1318
2. Trovarelli A, de Leitenburg C, Boaro M, Dolcetti G (1999) The utilization of ceria in industrial catalysis. *Catal Today* 50:353–367
3. Spanier JE, Robinson RD, Zhang F, Chan SW, Herman IP (2001) Size-dependent properties of CeO_{2-y} nanoparticles as studied by Raman scattering. *Phys Rev B* 64:245407
4. Tsunekawa S, Sahara R, Kawazoe Y, Kasuya A (2000) Origin of the blue shift in ultraviolet absorption spectra of nanocrystalline CeO_{2-x} particles. *Mater Trans JIM* 41:1104–1107
5. Bekyarova E, Fornasiero P, Kašpar J, Graziani M (1998) CO oxidation on $\text{Pd/CeO}_2\text{-ZrO}_2$ catalysts. *Catal Today* 45:179–183

6. Yahiro H, Baba Y, Eguchi K, Arai H (1988) High temperature fuel cell with Ceria-Yttria solid electrolyte. *J Electrochem Soc* 135:2077–2080
7. Li M, Zhang R, Zhang H, Feng W, Liu X (2010) Synthesis, structural and magnetic properties of CeO₂ nanoparticles. *Micro & Nano Letters* 5:95
8. Izu N, Shin W, Murayama N, Kanzaki S (2002) Resistive oxygen gas sensors based on CeO₂ fine powder prepared using mist pyrolysis. *Sensor Actuator B Chem* 87:95–98
9. Hirta Y, Harada A, Wang X (2005) Wet forming and sintering behavior of nanometer-sized ceria powder. *Ceram Int* 31:1007–1013
10. Chu X, Chung W-I, Schmidt LD (1993) Sintering of sol-gel prepared submicrometer particles studied by transmission electron microscopy. *J Am Ceram Soc* 76:2115–2118
11. Makishima A, Kubo H, Wada K, Kitami Y, Shimohira T (1986) Yellow coatings produced on glasses and aluminum by the sol-gel process. *J Am Ceram Soc* 69:C-127–C-129
12. Hakuta Y, Onai S, Terayama H, Adschiri T, Arai K (1998) Production of ultra-fine ceria particles by hydrothermal synthesis under supercritical conditions. *J Mater Sci Lett* 17:1211–1213
13. Uekawa N, Ueta M, Wu YJ, Kakegawa K (2004) Characterization of CeO₂ fine particles prepared by the homogeneous precipitation method with a mixed solution of ethylene glycol and polyethylene glycol. *J Mater Res* 19:1087–1092
14. Dong X, Hong G, Yu D, Yu D (1997) Synthesis and properties of cerium oxide nanometer powders by pyrolysis of amorphous citrate. *J Mater Sci Technol* 13:113–116
15. Masui T, Fujiwara K, Machida K-I, Adachi G-Y, Sakata T, Mori H (1997) Characterization of cerium(IV) oxide ultrafine particles prepared using reversed micelles. *Chem Mater* 9:2197–2204
16. Hsu WP, Ronnquist L, Matijevic E (1988) Preparation and properties of monodispersed colloidal particles of lanthanide compounds. 2. Cerium (IV). *Langmuir* 4:31–37
17. Chen P-L, Chen IW (1993) Reactive cerium(IV) oxide powders by the homogeneous precipitation method. *J Am Ceram Soc* 76:1577–1583
18. Liu K, Zhong M (2010) Synthesis of monodispersed nanosized CeO₂ by hydrolysis of the cerium complex precursor. *J Rare Earths* 28:680–683
19. Zhou XD, Huebner W, Anderson HU (2002) Room-temperature homogeneous nucleation synthesis and thermal stability of nanometer single crystal CeO₂. *Appl Phys Lett* 80:3814
20. Hessel V, Löwe H, Schönfeld F (2005) Micromixers—a review on passive and active mixing principles. *Chem Eng Sci* 60:2479–2501
21. Nguyen NT, Wu Z (2005) Micromixers—a review. *J Micromech Microeng* 15:R1
22. Schwarzer HC, Peukert W (2004) Tailoring particle size through nanoparticle precipitation. *Chem Eng Commun* 191:580–606
23. Chang CH, Liu SH, Tennico Y, Rundel JT, Remcho VT, Blackwell E, Tseng CH and Paul BK (2005) Progress towards chip-based high-throughput dendrimer synthesis. In: International Conference on Microreaction Technology. Atlanta, Georgia, pp. 3011–3018
24. Joanicot M, Ajdari A (2005) Droplet control for microfluidics. *Science* 309:887
25. Nakamura H, Yamaguchi Y, Miyazaki M, Maeda H, Uehara M, Mulvaney P (2002) Preparation of CdSe nanocrystals in a micro-flow-reactor. *Chem Commun* 23:2844–2845
26. Chan EM, Mathies RA, Alivisatos AP (2003) Size-controlled growth of CdSe nanocrystals in microfluidic reactors. *Nano Lett* 3:199–201
27. Yen BKH, Stott NE, Jensen KF, Bawendi MG (2003) A continuous-flow microcapillary reactor for the preparation of a size series of CdSe nanocrystals. *Adv Mater* 15:1858–1862
28. Krishnadasan S, Tovilla J, Vilar R (2004) On-line analysis of CdSe nanoparticle formation in a continuous flow chip-based microreactor. *J Mater Chem* 14:2655–2660
29. Ehrfeld W, Hessel V, Löwe H (2000) Microreactors: new technology for modern chemistry. Wiley, Weinheim
30. Tseng C, Paul B (2007) Comparison of batch mixing and micro-mixing approaches in the synthesis and deposition of ceria nanoparticles. *Trans NAMRI* 35
31. Chang H, Chen H (2005) Morphological evolution for CeO₂ nanoparticles synthesized by precipitation technique. *J Cryst Growth* 283:457–468
32. Yamashita M, Kameyama K, Yabe S, Yoshida S, Fujishiro Y, Kawai T, Sato T (2002) Synthesis and microstructure of calcia doped ceria as UV filters. *J Mater Sci* 37:683–687
33. Wang ZL, Feng X (2003) Polyhedral shapes of CeO₂ nanoparticles. *J Phys Chem B* 107:13563–13566
34. Tang C, Bando Y, Liu B, Golberg D (2005) Cerium oxide nanotubes prepared from cerium hydroxide nanotubes. *Adv Mater* 17:3005–3009
35. Mai H-X, Sun L-D, Zhang Y-W, Si R, Feng W, Zhang H-P, Liu H-C, Yan C-H (2005) Shape-selective synthesis and oxygen storage behavior of ceria nanopolyhedra, nanorods, and nanocubes. *J Phys Chem B* 109:24380–24385